Clinical & Experimental Metastasis (2023) 40:357–371
https://doi.org/10.1007/s10585-023-10219-5

RESEARCH PAPER

EGFL6 promotes bone metastasis of lung adenocarcinoma by increasing cancer cell malignancy and bone resorption

Xiaoting Song[1,2,3] · Xu Cheng[1,2,3] · Xiangang Jin[4] · Shengyu Ruan[1,2,3] · Xianquan Xu[1,2,3] · Feng Lu[4] · Xinhui Wu[1,2,3] · Fangying Lu[1,2,3] · Mingxuan Feng[5] · Liwei Zhang[1,2] · Renshan Ge[3] · Haixiao Chen[1,2] · Zhenghua Hong[1,2] · Dun Hong[1,2]

Received: 23 June 2022 / Accepted: 8 June 2023 / Published online: 28 June 2023

Abstract

Lung adenocarcinoma is the most common and aggressive type of lung cancer with the highest incidence of bone metastasis. Epidermal growth factor-like domain multiple 6 (EGFL6) is an exocrine protein, and the expression of EGFL6 is correlated with survival of patient with lung adenocarcinoma. However, the association between EGFL6 expression in lung adenocarcinoma and bone metastasis has not been investigated. In this study, we found that EGFL6 levels in lung adenocarcinoma tissues correlate with bone metastasis and TNM stages in surgical patients. In vitro, overexpression of *EGFL6* in lung adenocarcinoma cells promoted their proliferation, migration, and invasion ability compared with control by enhancing EMT process and activating Wnt/β-catenin and PI3K/AKT/mTOR pathways. In the nude mouse model, overexpression of *EGFL6* enhanced tumor growth and caused greater bone destruction. Moreover, the exocrine EGFL6 of human lung adenocarcinoma cells increased osteoclast differentiation of bone marrow mononuclear macrophages (BMMs) of mice via the NF-κB and c-Fos/NFATc1 signaling pathways. However, exocrine EGFL6 had no effect on osteoblast differentiation of bone marrow mesenchymal stem cells (BMSCs). In conclusion, high expression of *EGFL6* in lung adenocarcinomas is associated with bone metastasis in surgical patients. The underlying mechanism may be the increased metastatic properties of lung adenocarcinoma cells with high EGFL6 level and the enhanced osteoclast differentiation and bone resorption by exocrine EGFL6 from tumors. Therefore, EGFL6 is a potential therapeutic target to reduce the ability of lung adenocarcinomas to grow and metastasize and to preserve bone mass in patients with bone metastases from lung adenocarcinomas.

Graphical Abstract

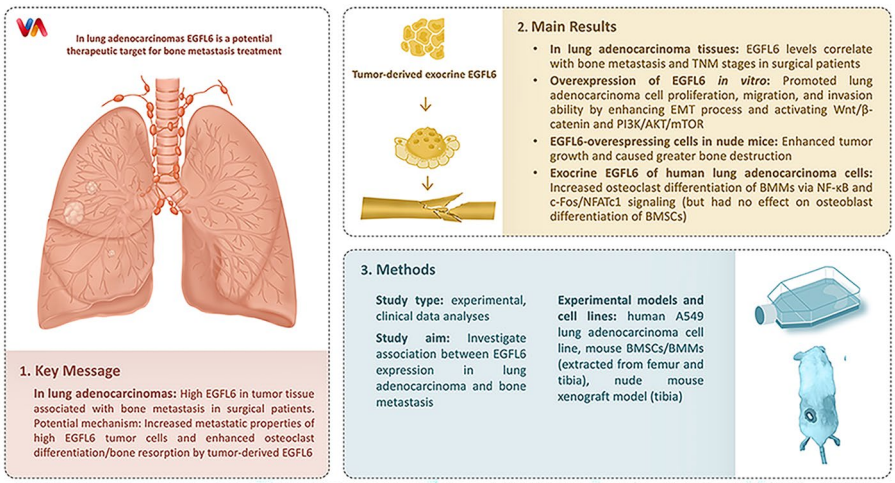

Extended author information available on the last page of the article

Keywords EGFL6 · Lung adenocarcinoma · Bone metastasis · EMT · Osteoclast differentiation

Abbreviations

BMMs	Bone marrow mononuclear macrophage
BMSCs	Bone marrow mesenchymal stem cells
CCK-8	Cell Counting Kit-8
EGFL6	Epidermal growth factor-like domain multiple 6
EMT	Epithelial mesenchymal transformation
IHC	Immunohistochemistry
M-CSF	Macrophage colonies stimulating factor
MCP1	Monocyte chemoattractant protein 1
NF-κB	Nuclear factor-kappa B
OPG	Osteoprotegerin
RANKL	Receptor activator of the NF-κB ligand

Introduction

Lung cancer is the leading cause of cancer deaths worldwide, among which lung adenocarcinoma is the most common and aggressive type [1, 2]. The skeletal system is one of the most common metastatic sites in lung cancer patients, accounting for approximately 30-40% of lung cancer patients [3, 4]. Bone metastasis patients often suffer skeletal-related events (SREs) including pathologic fractures, spinal cord compression, bone marrow aplasia, and hypercalcemia [5]. Among all types of lung cancer, lung adenocarcinoma has the highest incidence of bone metastasis [6].

The invasion of cancer cells into the bone microenvironment disrupts this normal bone remodeling process involving the osteoclast, osteoblast, and osteocyte [7]. The microenvironment in the development of bone metastasis should favor survival of the invading tumor cell [8]. For example, bone sialoprotein, a component of bone, has been shown to have predictive power for bone metastasis in resectable non-small-cell lung cancer [9, 10]. The receptor activator of nuclear factor-κB ligand (RANKL)/RANK/osteoprotegerin (OPG) system plays a pivotal role in bone remodeling by regulating osteoclast formation and activity. The expression of RANKL, RANK, and OPG was upregulated in primary non-small cell lung cancer (NSCLC) tissues with bone metastasis [11]. In addition, the macrophage-derived chemokine CCL22 produced by osteoclasts upregulated RANKL in osteoclast-like cells and promoted bone metastasis of lung cancer cells [12]. However, the underlying mechanism of bone metastasis in lung cancer, especially in lung adenocarcinoma, remains unclear.

Epidermal growth factor-like domain multiple 6 (EGFL6) is an exocrine protein and plays an important role in promoting endothelial cell migration and angiogenesis [13]. In a clinical study, cytoplasmic EGFL6 was found to be specifically expressed in lung adenocarcinomas, and patients younger than 69 years with high cytoplasmic EGFL6 expression had a lower 5-year survival rate and shorter median survival time compared with patients with low cytoplasmic EGFL6 [14]. Ectopic expression of EGFL6 has been shown to promote the cancer cell proliferation, migration, and invasion in breast, gastric, ovarian, colon, and nasopharyngeal cancers [15–19]. Since lung adenocarcinoma most frequently lead to bone metastasis [6], EGFL6 secreted by lung adenocarcinoma cells may affect the malignancy of lung adenocarcinoma and the activities of bone cells at the metastatic sites. However, the relationship between the expression of EGFL6 in lung adenocarcinoma and bone metastasis has not yet been investigated, either in terms of clinic aspect or the underlying mechanism.

In this study, we find that high expression of EGFL6 in lung adenocarcinoma tissues positively correlates with bone metastases and TNM stages of surgical patient. In addition, EGFL6 promotes bone metastasis of lung adenocarcinoma by increasing cancer cell malignancy and bone resorption. Our study shows that EGFL6 is a potential therapeutic target for the treatment of bone metastasis in lung adenocarcinoma.

Materials and methods

Specimen collection

We collected 30 lung adenocarcinoma tissues and matched adjacent normal tissues from the *Biological Resource Center of Enze Medical Center*, Taizhou Hospital. The specimens were staged according to the 8th manual of the American Joint Committee on Cancer Staging Manual [20]. The time distribution of patients undergoing lung surgery was from 2004 to 2012, and the clinical data and follow-up information of the patients were fully recorded. This study was approved by the Medical Ethics Committee of Taizhou Hospital, and the informed consent of all patients was obtained.

Immunohistochemistry (IHC)

Paraffin sections were baked in a 60 °C in an incubator at 60 °C for 2 h before processing, and then taken out and cooled to room temperature. After deparaffinization and rehydration, the tissue sections were heated with

citrate buffer to perform antigen retrieval in an autoclave. Then, 3% H_2O_2 was added to the slices to block endogenous peroxidase. Normal sheep serum (Gibco) was used to block nonspecific binding sites. The sections were incubated with anti-EGFL6 antibody (1:100, ab140079, Abcam, MA, USA) overnight. After that, the secondary antibody was added to the sections. Finally, the tissue sections were sequentially treated with hydrochloric acid, hematoxylin counterstain, dehydration, and sealing.

These sections were graded by professional pathologists and were based on the staining intensity of and the percentage of positively stained cells. The intensity was divided into four grades: 0 (negative), 1 (weak), 2 (medium) and 3 (strong). The percentage of positive staining cells was graded as follows: 1 (0–25%), 2 (26–50%), 3 (51–75%), and 4 (76–100%). We multiplied the two scores, the final score falling in the range of 0–6 was defined as low EGFL6 expression, and 7–12 was defined as high EGFL6 expression.

Cell culture

The human A549 and NCI-H292 lung adenocarcinoma cell lines were purchased from the Type Culture Collection of the Chinese Academy of Sciences (Shanghai, China). The authenticity of A549 cells and NCI-H292 cells has been verified using Short Tandem Repeat (STR) profiling within the last 3 years. A549 and NCI-H292 cells were cultured in RPMI 1640 medium containing 1% penicillin/streptomycin, 10% fetal bovine serum (FBS) (Gibco, Grand Island, NY, USA). Cells were maintained in an incubator at 37 °C with a humidity of 5% CO_2. All experiments were performed with cells without mycoplasma.

Cell transfection

For knockdown of EGFL6 in A549 and NCI-H292 cells, the siRNA targeting *EGFL6* (L-EGFL6) and the paired negative control (L-Ctrl) were synthesized by GenePharma (Shanghai, China). The sequences are as follows: L-EGFL6: sense 5'-GUUUCGAACUGCAAUAUAUAUTT-3' and antisense 5'-AUAUAUUGCAGUUCGAAACTT-3'; L-Ctrl: sense 5'-UUCUCCGAACGUGUCACGUTT-3' and antisense 5'-ACGUGACACGUUCGGAGAATT-3'. A549 cells were seeded in six-well plates and transfected with 5 µl siRNA and 5 µl Lipofectamine 2000 (Invitrogen).

As for the overexpression of EGFL6, the LV-EGFL6-RNAi (H-EGFL6) and control vector (H-Ctrl) was obtained from GeneChem (Shanghai, China). Cells were grown in 24-well plates and transfected with lentivirus and 20 µl HitransG according to the manufacturer's instructions.

Cell proliferation assay

Cell Counting Kit-8 (CCK-8, Dojindo, Japan) was used to measure cell proliferation ability. The cells were cultured into 96-well plates, and 10 µl CCK8 was added to each plate at 0, 24, 48, 72, 96 h. Then, after 2 h incubation at 37 °C, the determination of cell proliferation was replaced by the absorbance value at 450 nm.

Colony formation assay

The transfected cells were seeded in 6-well plates at a density of 1,000 cells per well. After culturing for 10d, the colonies were fixed with 4% paraformaldehyde for 30 min and then stained with 0.1% crystal violet for 30 min. The number of colonies was counted and compared in each group.

Migration and invasion assay

Cells were transfected on the 24-well trans-well plates (Corning Inc., Corning, NY). For migration assays, a serum free cell suspension (100 µl) containing 5×10^4 cells was added into the upper chamber, and medium containing 10% FBS was added to the lower chamber. After incubating for 12 h at 37 °C, the cells at the bottom of the upper chamber were fixed with 4% paraformaldehyde for 30 min and stained with 0.1% crystal violet for 30 min. Then, a cotton swab was used to remove the non-migrating cells in the upper chamber. For the invasion assay, the upper chamber was pre-coated with Matrigel (BD Biosciences, San Jose, CA), and the cell number of the cell suspension was changed to 1×10^5. The remaining steps were the same as the migration assay. Finally, we counted and compared the number of cells of each group.

Wound healing assay

The wound healing assay was performed by culturing insert (ibidi GmbH, Martinsried, Germany) in 24-well plates. The cell suspension (70 µl) at a density of 5×10^4 cells/ml was placed into each well of the culture-insert. After incubating at 37 °C and 5% CO2 for 24 h, we used sterile tweezers to gently remove the culture–insert and photographed under an optical microscope. Then, we added serum free RPMI 1640 medium (300 µl) to each well and cultured for 24 h. Time lapse images were captured at the same position at 0 and 24 h.

Immunocytochemistry

A cell suspension containing 1×10^4 cells was seeded on a coverslip in 12-well plates. After the cells were attached to the coverslips, they were fixed with 4% paraformaldehyde for 30 min. The cells were permeabilized in 0.5% Triton X-100 for 10 min, then blocked with 10% FBS for 30 min. The primary antibodies E-cadherin, N-cadherin, and Vimentin (CST, Beverly, MA, USA; diluted 1:250) were used to incubate with the cells overnight at 4 °C. On the next day, the cells were cultured with the fluorescently labeled secondary antibody (diluted 1:250) for 1 h in the dark. Later, the cells were stained with DAPI for 5 min and then mounted. Images were captured under confocal microscope.

Real-time PCR

Total RNA was extracted from transfected cells by TRIzol reagent (Invitrogen) following the manufacturer's instructions. Then, the total RNA was reverse transcribed into cDNA using the HiFiScript cDNA Synthesis Kit (CWBIO, Beijing, China). Quantitative real-time PCR analysis was performed by an ABI 7500 Real-Time PCR System (Applied Biosystems, Foster City, CA, USA) with ChamQ Universal SYBR qPCR Master Mix (Vazyme, China) in triplicate and the following cycling parameters: 40 cycles of 94°C for 30 sec; 60°C for 10 sec; 72°C for 30 sec. The *GAPDH* gene was utilized as housekeeping gene. All sequences were listed as follows: *EGFL6* (forward: 5'-CTCCTACCTGACCTGCAACC-3', reverse: 5'-GCCAGGGCATTGTTACTGTT-3'); *E-cadherin* (forward: 5'-GTCTCTCTCACCACCTCCACAG-3', reverse: 5'-CTCGGACACTTCCACTCTCTTT-3'); *N-cadherin* (forward: 5'-TGCTACTTTCCTTGCTTCTGAC-3', reverse: 5'-TAACACTTGAGGGGCATTGTC-3'); *Vimentin* (forward: 5'-GAAGAGAACTTTGCCGTTGAAG-3', reverse: 5'-GAAGGTGACGAGCCATTTC-3'); *MMP2* (forward: 5'-ACTGAGAGGCTCCGAGAAATG-3', reverse: 5'-GAACCCCGCATCTTGGCTT-3'); *MMP9* (forward: 5'-TGTACCGCTATGGTTACACTCG-3', reverse: 5'-GGCAGGGACAGTTGCTTCT-3'); *Snai1* (forward: 5'-TCGGAAGCCTAACTACAGCGA-3', reverse: 5'-AGATGAGCATTGGCAGCGAG-3'); *Slug* (forward: 5'-TGTGACAAGGAATATGTGAGCC-3', reverse: 5'-TGAGCCCTCAGATTTGACCTG-3').

Western blot

Total cellular protein of transfected cells was extracted using Radio-Immunoprecipitation Assay buffer (RIPA) containing protease inhibitor PMSF (100:1) and phosphatase inhibitor (Beyotime, Shanghai, China) (100:1). Quantitative of protein concentration was detected by BCA assay (Beyotime, Shanghai, China). The protein samples at the same quantity were separated by 10% SDS-PAGE and then transferred to PVDF membranes (Bio-Rad, Hercules, CA, USA). After blocking with Western Blocking Buffer (Biosharp, China) for 2 h, the PVDF membranes were incubated with primary antibodies: EGFL6, MMP2, MMP9 (1:1000, Abcam), E-cadherin, N-cadherin, Slug, Snail, Vimentin, p-GSK-3β, GSK-3β, β-catenin, p-PI3K, PI3K, p-AKT, AKT, p-mTOR, mTOR, c-Fos, NFATc1, p-ERK, ERK, p-JNK, JNK, p-p38, p38, GAPDH (1:1000, CST Beverly, MA, USA) at 4 °C overnight. The membranes were washed by TBS-Tween and incubated with HRP-conjugated secondary antibodies for 1 h at room temperature. Chemiluminescent HRP Substrate (Millipore Corporation, Billerica, MA, USA) and ImageQuant LAS 500 (GE Health Care, Fairfield, CT, USA) were used to observe the immunoreactivity. ImageJ software was utilized to quantify the intensity of the bands.

Measurement of EGFL6 concentration in the medium

An ELISA assay was used to verify whether EGFL6 play an exocrine role. The medium of the A549 lung adenocarcinoma cells cultured for 2d was extracted, and the concentration of EGFL6 was detected using an ELISA kit (AMEKO, China). The optical density was measured at 450 nm using the Multiskan FC Microplate Photometer (Thermo Fisher Scientific, Waltham, MA, USA). The standard curve with the OD value as the ordinate and standard concentration as the abscissa. The concentration of EGFL6 in each medium could be determined by the measured OD value against the standard curve.

Osteoclast differentiation

Bone marrow mononuclear macrophage (BMMs) were extracted from the femur and tibia of C57BL6 mice (8-week-old). After culturing for 4d or reaching 90% confluence in a 10 cm cell culture dish, the BMMs were seeded into a 96-well plate at a density of 8,000 cells/well in complete α-MEM containing 30ng/ml macrophage colonies stimulating factor (M-CSF). After 24 h, we replaced the medium with complete α-MEM containing 30ng/ml M-CSF and 50ng/ml RANKL and then added 50 μl/ml culture medium of L-Ctrl, L-EGFL6, H-Ctrl or H-EGFL6. The osteoclast induction medium was changed every 2d until the 7th day.

The BMMs were divided into the control and the rEGFL6 groups and inoculated in 96-well plates, and the above concentrations of M-CSF and RANKL were added for osteoclast differentiation. EGFL6 protein (MCE, China), derived from mouse, was added into the rEGFL6 group at the concentration of 1.33 mg/μl according to the manufacturer's instructions. The cells were fixed by 4% paraformaldehyde for 1 h, and then stained by TRAP activity kit (Sigma-Aldrich, St. Louis, MO, USA). ImageJ software was used to quantify the area (percentage of a well) of TRAP-positive cells (≥ 3 nuclei).

Osteoblast differentiation

Bone marrow mesenchymal stem cells (BMSCs) were extracted from the femur and tibia of C57BL6 mice (8 weeks old) and cultured in complete α-MEM for 6d or reached 90% confluence in a 10 cm cell culture dish. For osteoblast differentiation, BMSCs were re-seeded into a 12-well plate at a density of 1×10^4 cells/well with osteogenic medium (Complete DMEM supplemented with 10mM β-glycerophosphate, 50μM ascorbic acid and 100nM dexamethasone) and then added 50 μl/ml culture medium of L-Ctrl, L-EGFL6, H-Ctrl or H-EGFL6. The medium was changed every 2d. On day 7 and 21, the cells were stained with alkaline phosphatase (ALP), and the mineralized bone nodules were stained with Alizarin Red.

Bone absorption assay in vitro.

BMMs were seeded into 100 μm bovine bone slices (Rongzhi Haida Biotech Co., Ltd, Beijing, China) at a density of 1×10^4 cells/well in α-MEM supplemented with 100 ng/ml RANKL and the culture medium of L-Ctrl, L-EGFL6, H-Ctrl or H-EGFL6 respectively. The osteoclast induction medium was changed every 2d until the 14th day. The cells were eliminated by mechanical agitation and sonication. Then, the resorption pits were examined by scanning electron microscope (Field Environmental Instruments Inc., Hillsboro, OR). ImageJ software was utilized to quantify the area of resorption pits.

Nude mouse tumor-induced bone destruction model in vivo.

All animal experiments followed the guidance of the Institutional Animal Ethics Committee of Taizhou Hospital. 6-week-old female nude mice were randomly divided into L-Ctrl, L-EGFL6, H-Ctrl and H-EGFL6 group (6 mice/group). After induction of anesthesia, 20 μl of transfected tumor cells (1×10^6 cells/ml) suspended in Phosphate Buffered Saline (PBS) were injected into the tibial marrow cavity through the tibial plateau of nude mice. All mice were euthanized on day 14. We removed the hind limbs of nude mice and compared the size of tumor. Then, the hind limbs were fixed in 4% paraformaldehyde and collected for further experiments.

Histological and histomorphometric analysis

After decalcification in 10% EDTA (ethylenediaminetetraacetic acid) for 14d, the fixed hind limbs were embedded in paraffin and then sectioned. The tissue slices were utilized for H&E and TRAP staining. We acquired images of each sample through a high-quality microscope (Olympus, Japan) and counted the number of TRAP-positive cells in each sample.

Statistical analysis

The significant differences between groups were analyzed by Student's t-test or one-way ANOVA or Kruskal Wallis test using GraphPad Prism® version 8.3.1. All in vitro experiments were performed independently at least 3 times. The relationship between the expression of EGFL6 and clinicopathological indexes was analyzed by $\chi 2$ or Fisher's Exact Test by IBM SPSS Statistics 26.0 for Mac (IBM Corp, Armonk, NY, USA). Results were presented as mean ± SD. $P < 0.05$ was considered statistically significant.

Results

The expression of EGFL6 is elevated in lung adenocarcinoma patients with bone metastasis

The expression of EGFL6 in lung adenocarcinoma tissues was higher than in adjacent normal tissues (Fig. 1). The percentage of high-grade expression of EGFL6 was greater in older patients (≥ 60 years) than in younger patients (< 60 years) (p = 0.023) and was also greater in stage I and II patients than stage III, IV patients (P = 0.004). In addition, all 10 patients with bone metastasis had high-grade expression of EGFL6 of lung adenocarcinoma, compared with the percentage of high-grade expression of EGFL6 in patients without bone metastasis (p = 0.011). However, the percentage of high-grade expression of EGFL6 was not significantly related to the histological grade and lymph node metastasis of the patients (Table 1).

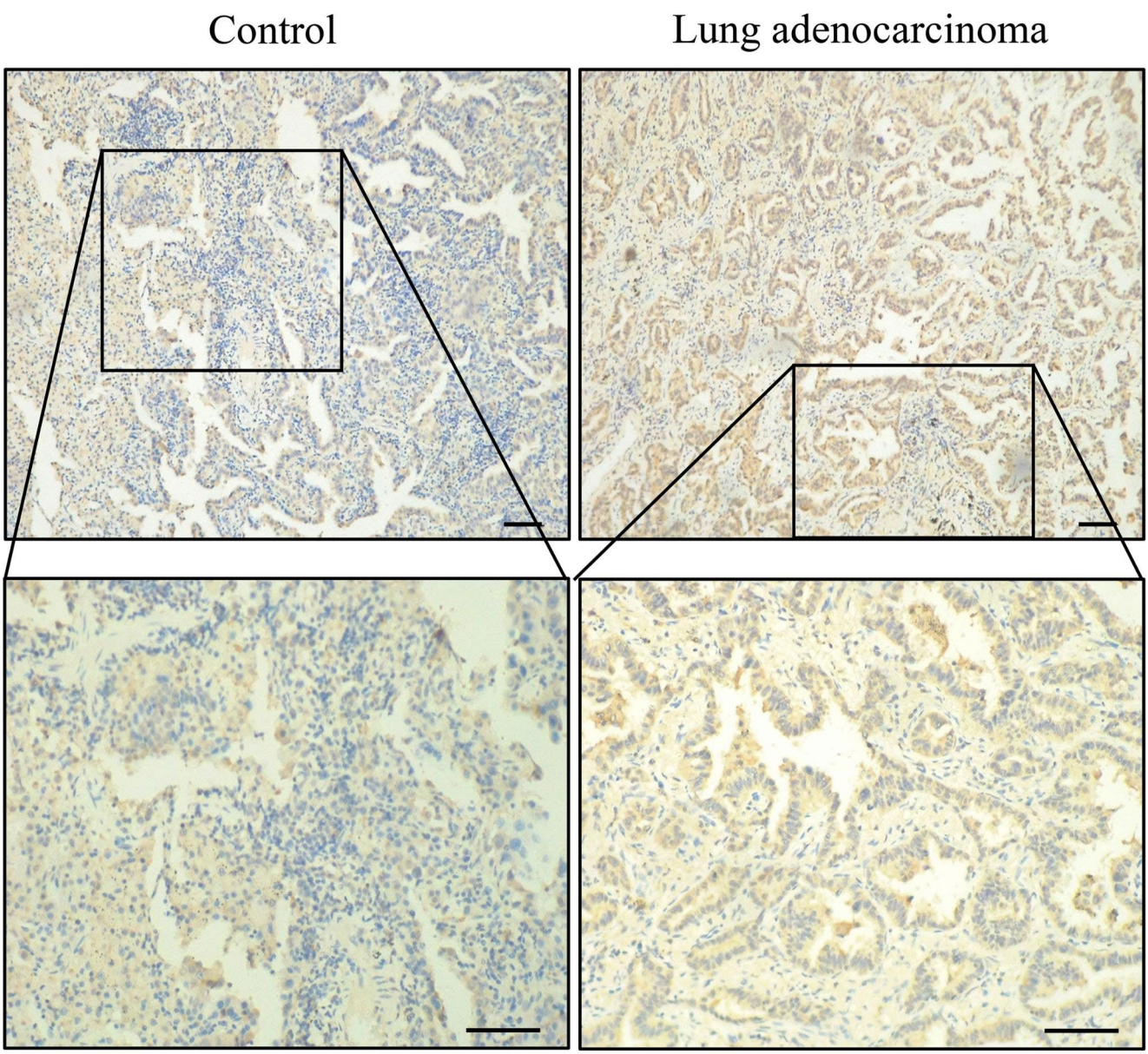

Fig. 1 EGFL6 is upregulated in lung adenocarcinoma tissues. The images of EGFL6 IHC staining in lung adenocarcinoma tissues and adjacent matched tissues. Scale bar represents 100 μm

Overexpression of EGFL6 increases proliferation, migration, and invasion of lung adenocarcinoma cells via activating EMT and Wnt, PI3K/AKT/mTOR signaling pathways

A549 and NCI-H292 cells obtained overexpression (H-EGFL6) and knockdown (L-EGFL6) of EGFL6 phenotypes under lentivirus and siRNAs respectively. The cells transfected with null vectors (H-Ctrl and L-Ctrl) were used as the control. The transfect efficiency were confirmed by WB, RT-PCR, and fluorescent staining (Fig. S1 a-h).

CCK8 assays demonstrated that overexpression of *EGFL6* significantly promoted the proliferation of A549 and NCI-H292 cells, whereas silencing *EGFL6* weakened the viability of cells (Fig. 2a, b). The colony formation assays also showed the same trend with CCK-8 (Fig. 2c). In addition, the number of migrated and invading cells in the *EGFL6* overexpression group was significantly greater than the control group (Fig. 2d, e). On the contrary, the *EGFL6* knockdown group had the opposite phenomenon. In addition, the cell scratch experiment found that the healing speed of the *EGFL6* overexpression group was significantly faster than that of the control

Table 1 The relationship between EGFL6 levels and clinicopathologic characteristics in lung adenocarcinomas

	Number (n = 30)	EGFL6 expression		*P* value
		High (%)	Low (%)	
Age (Year)				
≤ 60	13	5	8	**0.023**[*]
> 60	17	14	3	0.132
Gender	17	13	4	
Male	13	6	7	
Female				
Histological grades				
G1, G2	23	14	9	0.372
G3	7	6	1	
Lymph node metastasis				
Absent	17	10	7	0.440
Present	13	10	3	
TNM stage				
I, II	12	4	8	**0.004**[**]
III, IV	18	16	2	
Bone metastasis				
Absent	20	10	10	**0.011**[*]
Present	10	10	0	

[#] $\chi 2$; $P < 0.05$ are shown in bold, [*]$P < 0.05$, [**]$P < 0.01$

group, and depleting *EGFL6* expression slowed down the healing rate (Fig. 2f, g).

EMT is an important biological process for lung adenocarcinoma cells to acquire the ability of migration and invasion. RT-PCR showed that the forced expression of *EGFL6* up-regulated the mRNA level of *N-cadherin*, *Vimentin*, *MMP2*, *MMP9*, *Snail* and *Slug* while down-regulating the mRNA level of *E-cadherin*. Interference with *EGFL6* indicated the opposite results (Fig. 3a). The results of RT-PCR were further confirmed by WB (Fig. 3b). In addition, immunocytochemistry (ICC) confirmed that A549 cells overexpressing EGFL6 increased the expression of N-cadherin and Vimentin and reduced the expression E-cadherin, whereas silence of EGFL6 decreased the expression of N-cadherin and Vimentin and increased the expression of E-cadherin (Fig. 3c).

Wnt/β-catenin signaling pathway and PI3K/Akt/mTOR signaling pathway both play key roles in regulating the process of proliferation, migration, and invasion of tumor cells. The results of WB showed that the protein levels of GSK-3β and β-catenin were increased by overexpression of EGFL6 and decreased by silencing of EGFL6 (Fig. 4a, b). Moreover, the phosphorylation levels of PI3K, AKT and mTOR were increased by overexpression of EGFL6 and decreased by silencing EGFL6, while EGFL6 expression reduction had no significant effect on the phosphorylation level of mTOR, with no difference in total protein level (Fig. 4c, d).

EGFL6 increases tumor growth and bone destruction in tibia of nude mice invaded by lung adenocarcinoma cells

The suspensions of A549 cells of *EGFL6* overexpression, knockdown, and their respective control were injected into nude mice through the tibial plateau. After 14d, all nude mice were euthanized. In general, A549 cells overexpressing *EGFL6* formed larger tumors in the tibia of mice than control, while knockdown of *EGFL6* exhibited the opposite result (Fig. 5a, b). The X-ray images confirmed that cells overexpressing *EGFL6* resulted in greater loss of percentage bone volume to tissue volume (BV/TV), whereas cells with silencing expression of *EGFL6* showed the opposite result (Fig. 5c, d). The above result of tibial destruction was also confirmed by H&E staining (Fig. 5e, f). In addition, TRAP staining showed that A549 cells overexpressing *EGFL6* increased the number of osteoclasts and the number of TRAP-positive osteoclasts per bone surface (OCs/BS), whereas A549 cells with silencing expression of *EGFL6* decreased the number of osteoclasts and OCs/BS (Fig. 5g, h).

EGFL6 promotes osteoclast differentiation of BMMs and bone resorption by activating NF-κB and downstream c-Fos/NFATc1 signaling pathways

We verified that EGFL6 could be detected as an exocrine protein in the culture medium of A549 cells (Fig. 6a). The concentration of EGFL6 in the medium was higher in H-EGFL6 group than in H-Ctrl group and lower in L-EGFL6 group than in L-Ctrl group (Fig. 6a). The culture medium of A549 cells with different EGFL6 were harvested and added to the culture media of BMMs and BMSCs from 8-week-old mice. The media containing a higher concentration of EGEL6 secreted by A549 cells increased osteoclast differentiation of BMMs (Fig. 6d, e), but had no significant effect on osteoblast differentiation of BMSCs (Fig. 6b, c). Besides, EGFL6 protein, derived from mouse, promoted the osteoclast differentiation of BMMs (Fig. 6f, g). In vitro resorption assay of bovine bone showed that media with a higher concentration of EGEL6 secreted by A549 cells increased the bone resorption capacity of BMMs, whereas media with a lower concentration of EGEL6 weakened the capacity (Fig. 6h).

The WB results showed that the expression of c-Fos and NFATc1 during the osteoclast differentiation was significantly higher under the stimulation of RANKL and the medium of A549 cells (H-EGFL6) containing a higher concentration of EGEL6 at day 5 compared with control (L-Ctrl) (Fig. 7a). We also examined the short-term signaling pathways of MAPKs, NF-κB, and AKT

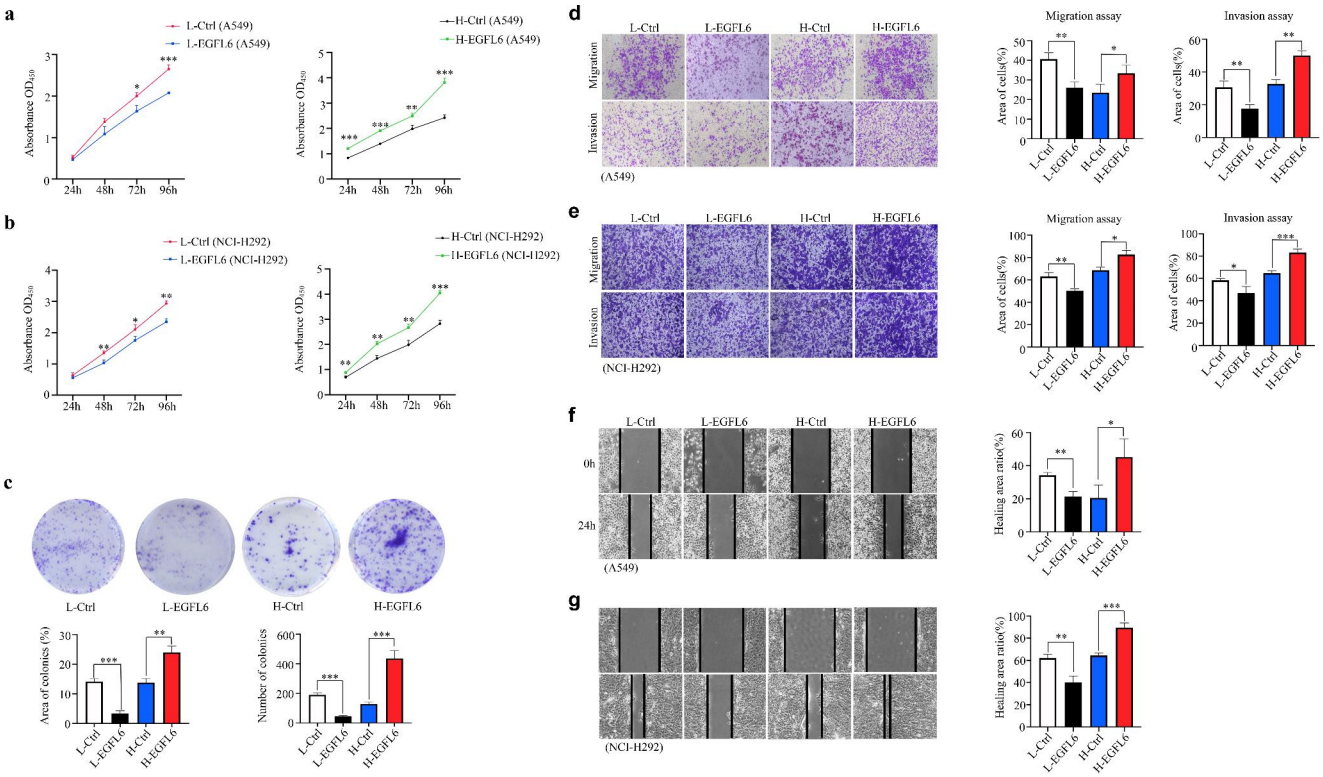

Fig. 2 EGFL6 promotes the proliferation, migration, and invasion of lung adenocarcinoma A549 cells. Knockdown of EGFL6 is expressed as Low-EGFL6 (L-EGFL6), and the relative control is expressed as Low-Ctrl (L-Ctrl). Overexpression of EGFL6 is expressed as High-EGFL6 (H-EGFL6), and the relative control is expressed as High-Ctrl (H-Ctrl). (**a,b**) CCK-8 analysis shows that overexpression of EGFL6 significantly promotes the proliferation of A549 and NCI-H292 cells, knockdown of EGFL6 weakens this ability. (**c**) Colony formation assay exhibits the same results of CCK-8. (**d,e**) Trans-well assay displays that overexpression of EGFL6 increases the migration and invasion of A549 and NCI-H292 cells while knockdown of EGFL6 reveals the opposite. (**f,g**) Testing the rate of wound closure indicates that overexpression of EGFL6 promotes the cell mobility in A549 and NCI-H292 cells, knockdown of EGFL6 attenuates the migration ability. Results were presented as mean ± SD. $P < 0.05$ was considered statistically significant. $^{*}P < 0.05$, $^{**}P < 0.01$, $^{***}P < 0.001$

in the H-EGFL6 and L-Ctrl groups. As shown in Fig. 7b, exocrine EGFL6 did not influence the phosphorylation levels of AKT and MAPK members ERK, JNK and p38 in BMMs. In contrast, exocrine EGFL6 increased the phosphorylation of NF-κB member IκBα at 10 min (Fig. 7c).

Discussion

In this study, we found that high-grade expression of EGFL6 in specimens of lung adenocarcinoma was highly associated with age (> 60 years), bone metastasis and III, IV TNM stages. Our clinicopathological finds were contrast with a retrospective study, which showed that the immunoreactivity levels of EGFL6 in lung adenocarcinoma samples were not correlated with age, gender, grade, and TNM stages [14]. This retrospective study indicated that high EGFL6 expression might serve as a marker of poor clinical outcome of lung adenocarcinoma, especially in younger patients [14]. For many tumor cells such as lung, breast, and prostate cancer cells, bone is the preferred site of metastasis [21–23]. Since the overall survival of lung adenocarcinoma patients with bone metastasis was significantly shorter than that of patients without bone metastasis, it is important to predict the occurrence of bone metastasis early in patients with lung adenocarcinoma [24, 25]. Our study showed that all lung adenocarcinoma samples from patients with bone metastasis had high-grade EGFL6 expression, suggesting that lung adenocarcinoma patients with high-grade EGFL6 expression should be closely monitored for possible bone metastasis.

The model, created by direct inoculation of tumor cells into bone, mimics the late phase of the bone metastasis [26]. This modeling approach has the advantage of studying the interaction between tumor cells and bone tissue. Our in vivo study in mice showed that lung adenocarcinoma cells overexpressing EGFL6 formed larger tumors and caused more severe bone destruction in the tibia of nude mice. It is well accepted that EGFL6 plays an important role in the formation of new blood vessels of epithelial cells, which is a necessary process for tumor

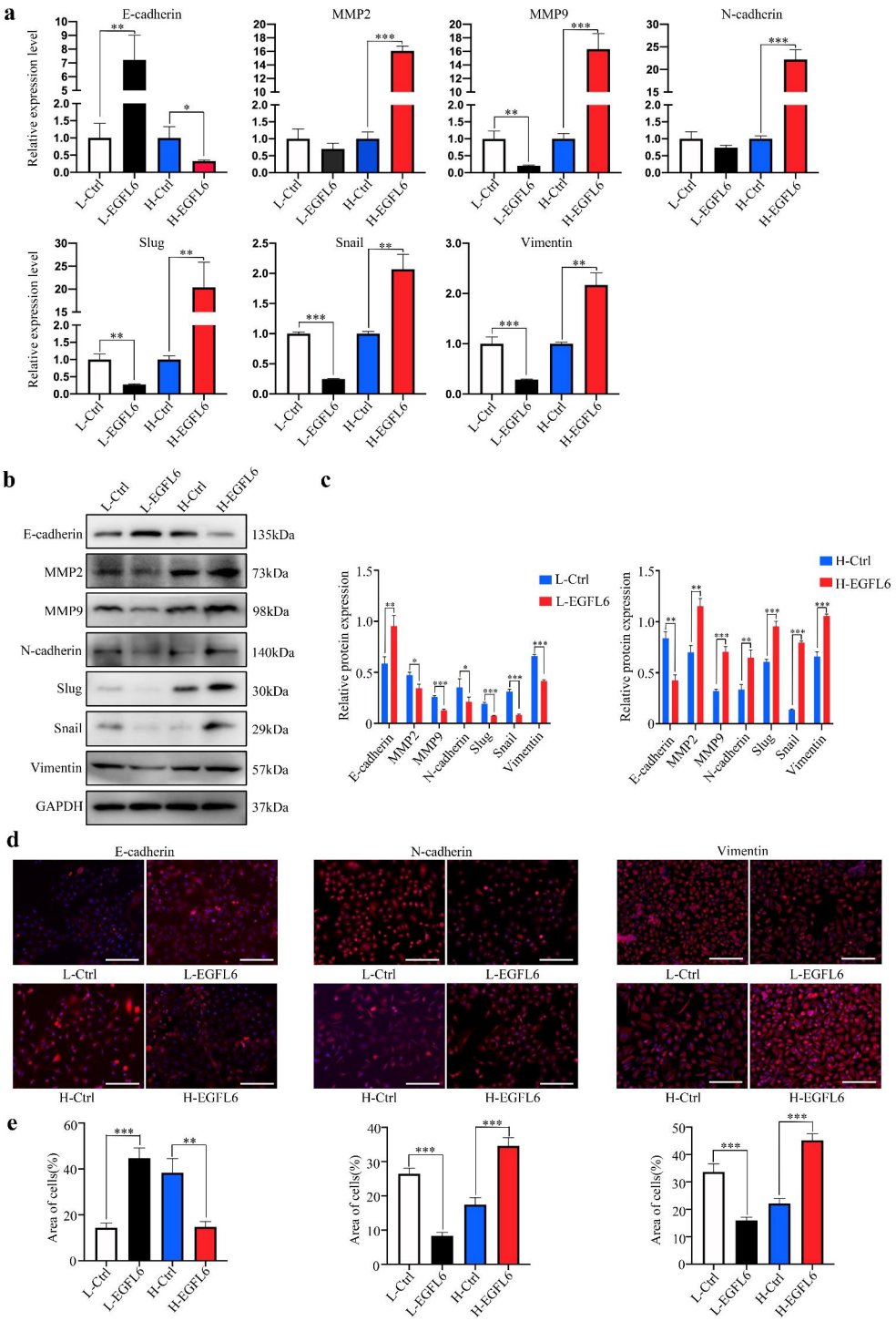

Fig. 3 Effects of EGFL6 on EMT-related gene expression. (**a**) RT-PCR shows that overexpression of *EGFL6* promotes the expression of *N-cadherin*, *MMP2*, *MMP9*, *Vimentin*, *Snail*, and *Slug* and down-regulates the expression of *E-cadherin*. Knockdown of *EGFL6* exhibits the opposite results. (**b,c**) Western blot replicates the RT-PCR results. (**d,e**) The effect of EGFL6 on EMT markers (E-cadherin, N-cadherin, and Vimentin) in A549 cells is detected by ICC. Over-expression of EGFL6 increases the expression of N-cadherin and Vimentin in cytoplasm but attenuates the expression of E-cadherin while knockdown of EGFL6 displays the adverse. Results were presented as mean ± SD. $P < 0.05$ was considered statistically significant. *$P < 0.05$, ** $P < 0.01$, *** $P < 0.001$

growth and metastasis [13, 19, 27, 28]. Interestingly, we observed that the number of osteoclasts was increased in the tibia of nude mice under the invasion of lung adenocarcinoma cells with high EGFL6 expression. Our study showed that EGFL6 protein or secreted by lung adenocarcinoma cells could both increase osteoclast differentiation and bone resorption of BMMs. Besides, in Fig. 5c, burr-like new bone formation was seen in the tumor on X-ray, indicating that EGFL6 overexpression promoted bone destruction while also promoting bone formation to some extent. As we all know, bone remodeling includes both bone formation and bone destruction processes. The results of X-ray, in addition with no effect on osteoblast differentiation in vitro of EGFL6, might indirectly demonstrate that EGFL6 could promote the osteoclast differentiation and the process of bone remodeling.

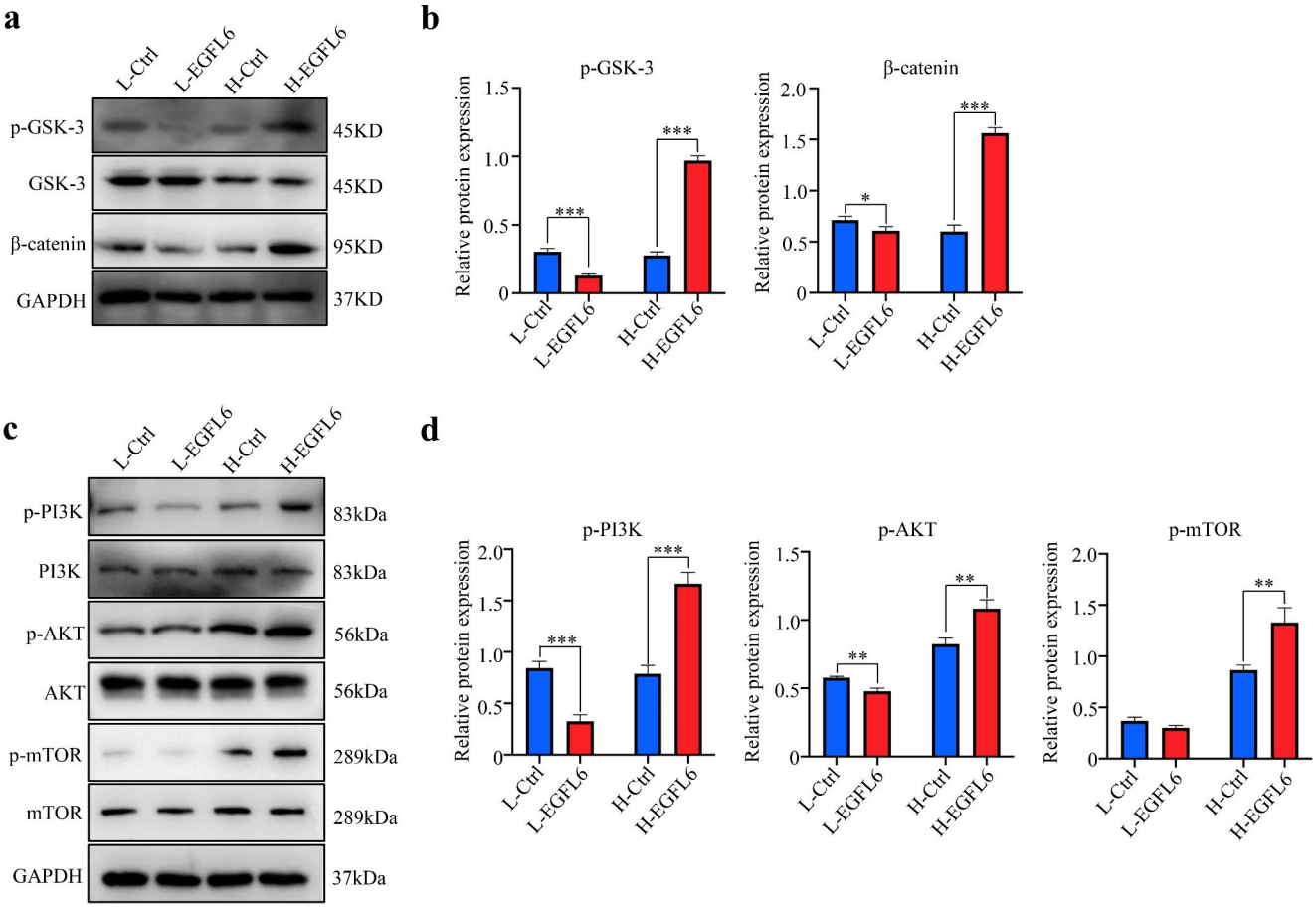

Fig. 4 EGFL6 enhanced the Wnt and PI3K/AKT/mTOR signaling pathways of lung adenocarcinoma A549 cells. (**a,b**) Western blotting analysis is utilized to detect the levels of p-GSK-3β, GSK-3β and β-catenin under the influence of overexpression and knockdown of EGFL6 in A549 cells. (**c,d**) Western blotting analysis is utilized to detect the levels of p-PI3K, PI3K, p-AKT, AKT, p-mTOR and mTOR under the influence of over-expression and knockdown of EGFL6 in A549 cells. Results were presented as mean ± SD. $P < 0.05$ was considered statistically significant. $^{*}P < 0.05$, $^{**}P < 0.01$, $^{***}P < 0.001$

We found that EGFL6 increased the expression of c-Fos and NFATc1, which play an essential role in the downstream pathways of osteoclast differentiation [29, 30]. EGFL6 increased osteoclast differentiation not through the MAPKs and AKT signaling pathways but through the traditional NF-κB signaling pathway, in which phosphorylation of IκBα causes nuclear translocation of p65 and eventually leads to NF-κB activation [31]. Therefore, future studies are needed to find molecules targeting EGFL6 or the NF-κB pathway to reduce bone resorption induced by metastatic lung adenocarcinoma.

Our in vitro studies have also shown that overexpression of EGFL6 promotes the proliferation, migration, and invasion of lung adenocarcinoma cells through enhanced EMT process and activation of Wnt/β-catenin and PI3K/AKT/mTOR pathways. EMT gives tumor cells the characteristics of metastasis, accompanied by the decrease of epithelial markers and the increase of mesenchymal markers [32]. As a complex biological process of tumorigenesis and progression, EMT is regulated by a variety of signaling pathways, like Wnt/β-catenin [33], PI3K/AKT/mTOR [34], MAPK [35], and Notch [36]. In Wnt/β-catenin signaling pathway, cytoplasmic β-catenin is degraded by glycogen synthase kinase 3β (GSK3β). Our study showed that overexpressing EGFL6 promoted the phosphorylation levels of GSK3β and β-catenin in lung adenocarcinoma cells, while silencing EGFL6 showed the opposite effect. Furthermore, hyperactivation of PI3K signaling pathway can regulate cell movement, survival, growth, and metabolism in human cancers, like ovarian, gastric, breast and prostate cancers [37–41]. In our study, overexpression of EGFL6 increased the expression of p-PI3K, p-AKT, and p-mTOR in lung adenocarcinoma cells. It is worthwhile to explore deeper of the mechanism by which EGFL6 exerts its effect, which may be a common downstream signaling molecule of Wnt/β-catenin and PI3K/Akt/mTOR signaling pathways and also involved in the EMT process. Currently, inhibitors

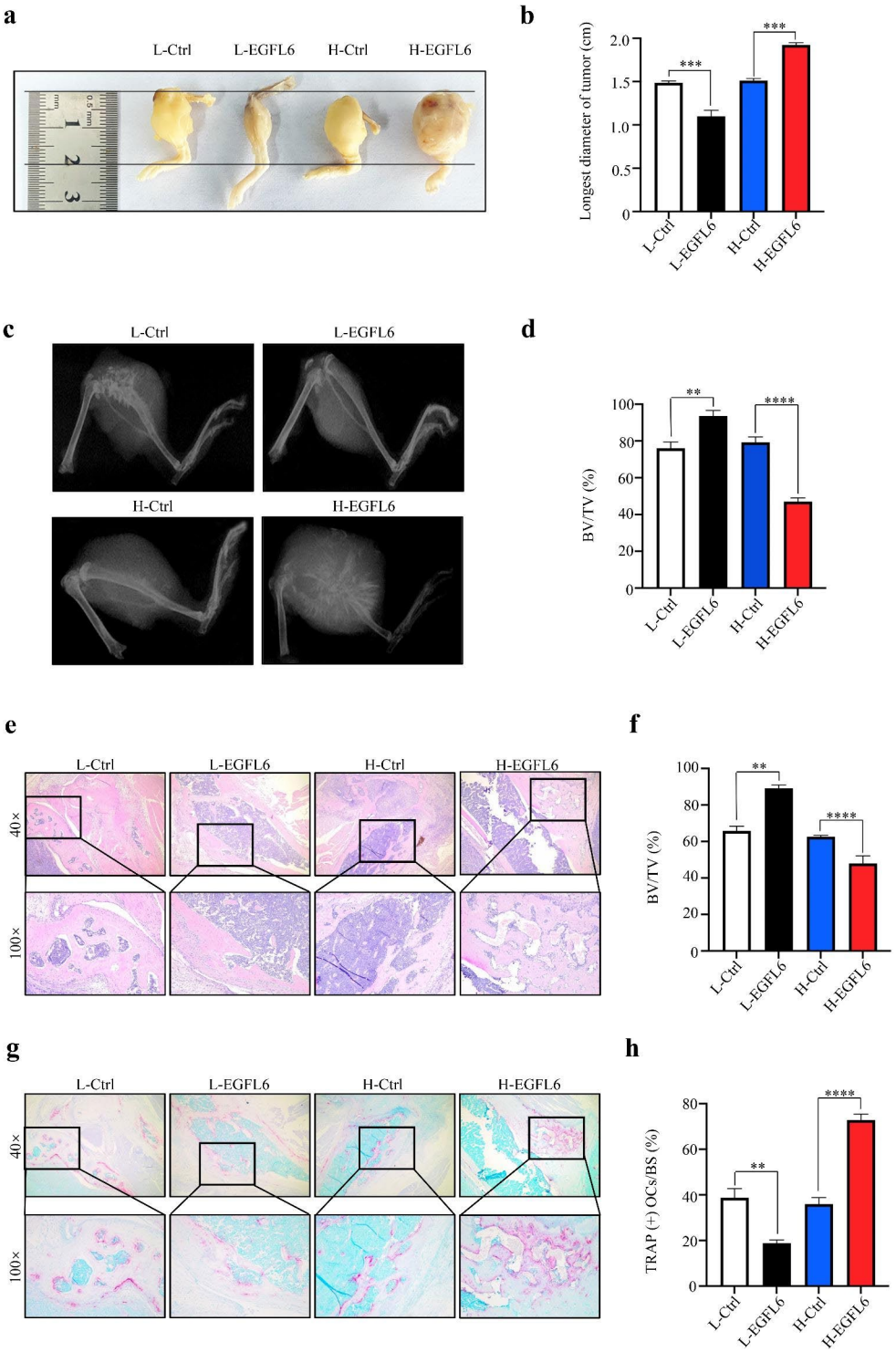

Fig. 5 EGFL6 moderates the effect of A549 cells on skeleton system of nude mice and enhances the osteoclast differentiation of BMMs. (**a,b**) The tumor size in the H-EGFL6 group is much larger than the H-Ctrl group, and the L-EGFL6 group exhibited a smaller size than the L-Ctrl group. (**c**) Compared with each control, X-ray shows that the bone destruction of tibia in H-EGFL6 group is much severe, while in L-EGFL6 group is slight. (**d**) Histomorphometric quantitative analysis of percentage bone volume to tissue volume (BV/TV, %). (**e,f**) The tibial tumor sections of nude mice were stained with H&E. (**g**) The tibial tumor sections of nude mice were stained with TRAP. (**h**) The number of TRAP-positive osteoclasts per bone surface (OCs/BS). Results were presented as mean ± SD. $P < 0.05$ was considered statistically significant. $^{*}P < 0.05$, $^{**}P < 0.01$, $^{***}P < 0.001$

targeting PI3K, AKT, and mTOR in lung cancer are under various phases of clinical trials [42]. For example, onatasertib is an mTOR inhibitor and can reduce tumor growth by 47% in a patient-derived lung adenocarcinoma xenograft [43]. Our study suggested that molecules targeting EGFL6 might inhibit Wnt/β-catenin and PI3K/AKT/mTOR, thereby reduce bone metastasis.

There are still some limits in this study. First, subsequent experiments need to expand the number of lung adenocarcinoma samples to further confirm the clinical features of EGFL6. Second, bone metastasis samples of lung adenocarcinoma should be collected and examined for EGFL6 expression. Third, the angiogenesis role of EGFL6 on bone destruction and tumor growth in mice is

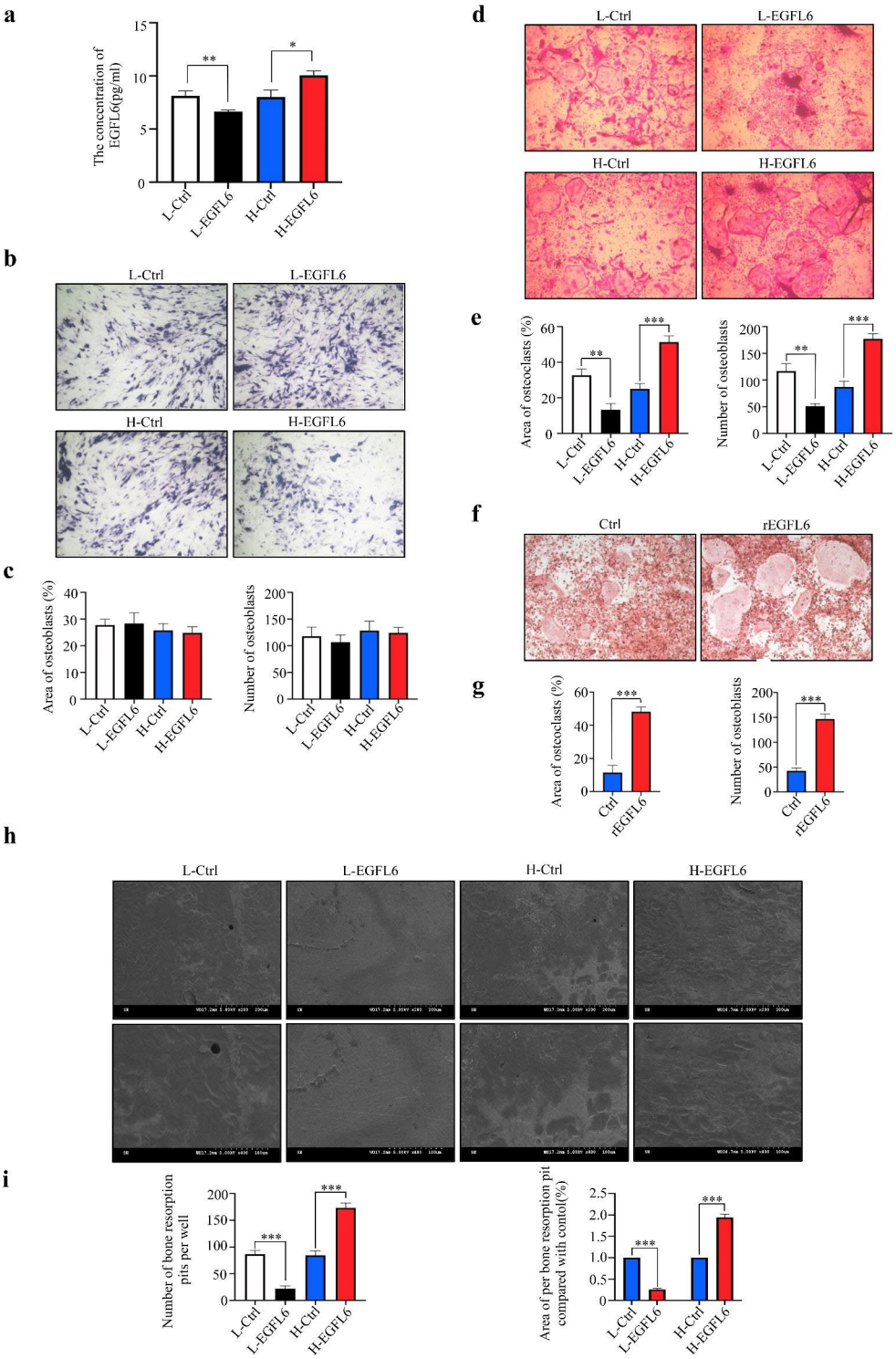

Fig. 6 EGFL6 promotes osteoclast differentiation of BMMs but has no significant effect on osteoblast differentiation of BMSCs as an exocrine protein. (**a**) ELISA assay shows that EGFL6 is an exocrine protein. (**b,c**) EGFL6 has no significant influence on osteoblast differentiation of BMSCs. (**d,e**) EGFL6 enhances the osteoclast differentiation of BMMs. (**f,g**) EGFL6 protein promotes the osteoclast differentiation. (**h,i**) The bone resorption pits assay. Results were presented as mean ± SD. $P < 0.05$ was considered statistically significant. $^{*}P < 0.05$, $^{**}P < 0.01$, $^{***}P < 0.001$

lacking. Finally, we have only shown in cellular experiments and clinical samples that EGFL6 promotes lung adenocarcinoma cell metastasis, and animal models of lung adenocarcinoma bone metastasis are needed for further validation.

In summary, our findings provide evidence that patients with lung adenocarcinoma who have high-grade expression of EGFL6 are at higher risk of bone metastasis and should be closely followed up. Overexpression of EGFL6 increases the proliferation, migration, and invasion ability of lung adenocarcinoma cells by promoting EMT, Wnt and PI3K/AKT/mTOR signaling pathways. Furthermore, overexpression of EGFL6 in lung adenocarcinoma cells increases osteoclast differentiation, bone

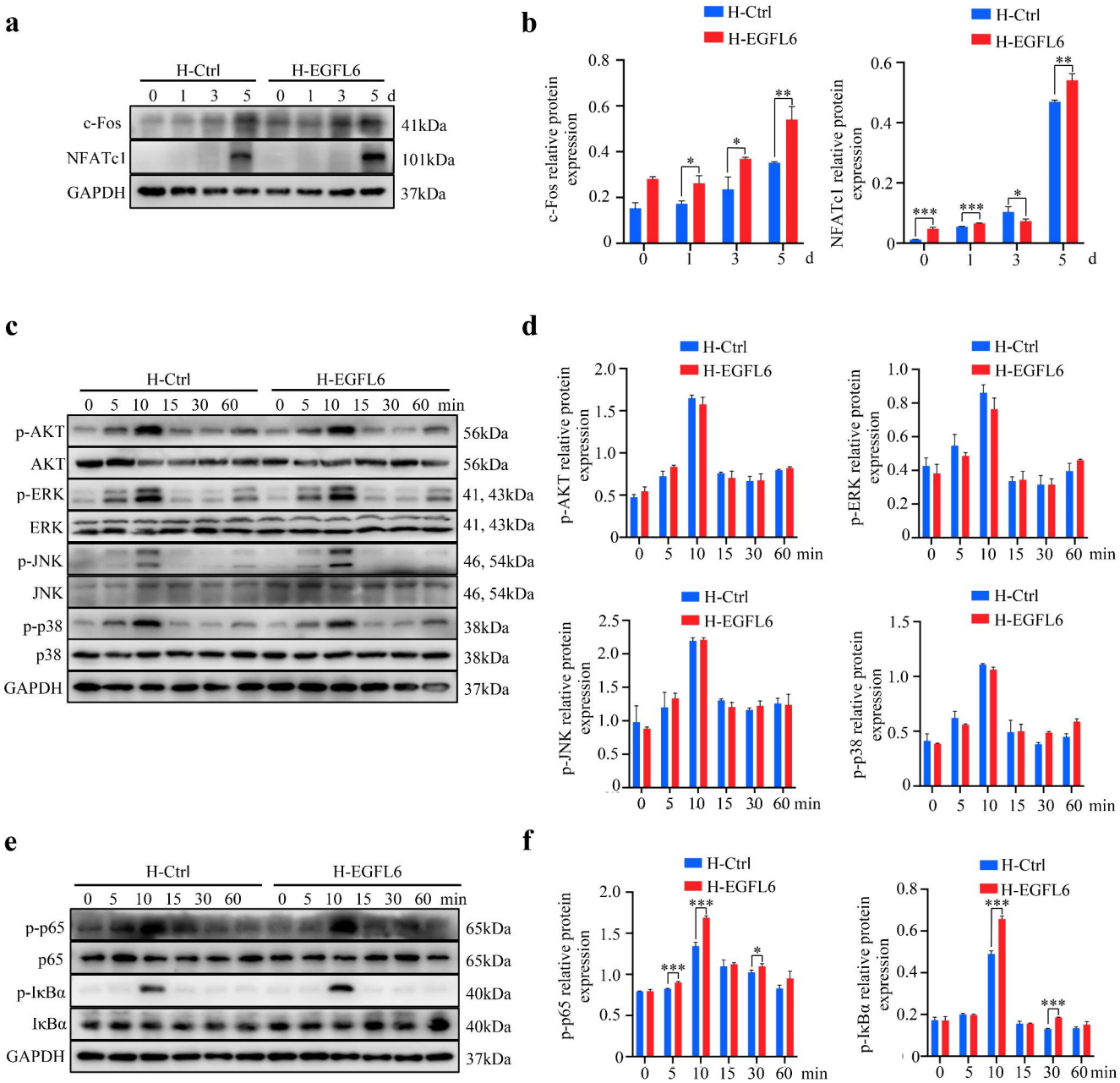

Fig. 7 Exocrine EGFL6 promotes osteoclast differentiation by activating the NF-κB and the downstream c-Fos/NFATc1 signaling pathway. (**a,b**) The expression of c-Fos and NFATc1 is detected by western blotting on day 0, 1, 3, and 5 under the effect of medium extracted from H-EGFL6 group, L-EGFL6 group and each control. (**c,d**) The expression of the phosphorylated or nonphosphorylated forms of AKT and MAPKs, including ERK, JNK and p38 kinase is detected by western blotting at different time points. (**e,f**) The expression of p-p65, p65, p-IκBα and IκBα is detected by western blotting at different time points. Results were presented as mean ± SD. $P < 0.05$ was considered statistically significant. $^{*}P < 0.05$, $^{**}P < 0.01$, $^{***}P < 0.001$

resorption, and bone destruction in mice by NF-κB signaling pathway. Therefore, we speculate that EGFL6 tends to be a future therapeutic target for the treatment of bone metastasis caused by lung adenocarcinoma.

Supplementary Information The online version contains supplementary material available at https://doi.org/10.1007/s10585-023-10219-5.

Acknowledgements We highly appreciated the patient samples provided by the Biological Resource Center of Enze Medical Center, Taizhou Hospital, and the support of Taizhou Discipline Group Fund.

Author contributions Dun Hong and Zhenghua Hong designed the study. The material preparation was performed by Xu Cheng, Xianquan Xu and Shengyu Ruan. Xinhui Wu, Feng Lu and Fangying Lu collected and analyzed the data. The animal experiment was conducted by Xiangang Jin and Mingxuan Feng. The first draft was written by Xiaoting Song. Review and editing were performed by Dun Hong,

Zhenghua Hong, Renshan Ge and Haixiao Chen. All authors read and approved the final manuscript.

Funding This work was supported by the Medical and Health Science and Technology Program Project of Zhejiang Province for Dun Hong, Grant/Award Number: 2020PY030; the Basic and Public Research Project of Zhejiang Province for Mingxuan Ming, Grant/Award Number: LGF19H070003.

Data Availability The data used to support the findings of this study are available from the corresponding author upon request.

Declarations

Competing interests The authors declare no competing interests.

Ethics approval This research was approved by the *Medical Ethics Committee of the Taizhou Hospital* and obtained the informed consent of all patients. All experiments of animal followed the instruction of the Institutional Animal Ethics Committee of Taizhou Hospital.

References

1. Siegel RL, Miller KD, Jemal A (2020) Cancer statistics, 2020. CA Cancer J Clin 70(1):7–30
2. Zhang H, Guo L, Chen J (2020) Rationale for Lung Adenocarcinoma Prevention and Drug Development based on Molecular Biology during Carcinogenesis. Onco Targets Ther 13:3085–3091
3. Cho YJ, Cho YM, Kim SH, Shin KH, Jung ST, Kim HS (2019) Clinical analysis of patients with skeletal metastasis of lung cancer. BMC Cancer 19(1):303
4. Bienz M, Saad F (2015) Management of bone metastases in prostate cancer: a review. Curr Opin Support Palliat Care 9(3):261–267
5. Macedo F, Ladeira K, Pinho F, Saraiva N, Bonito N, Pinto L, Goncalves F (2017) Bone Metastases: An Overview Oncol Rev 11(1):321
6. Yang M, Sun Y, Sun J, Wang Z, Zhou Y, Yao G, Gu Y, Zhang H, Zhao H (2018) Differentially expressed and survival-related proteins of lung adenocarcinoma with bone metastasis. Cancer Med 7(4):1081–1092
7. Yin JJ, Pollock CB, Kelly K (2005) Mechanisms of cancer metastasis to the bone. Cell Res 15(1):57–62
8. Wood SL, Pernemalm M, Crosbie PA, Whetton AD (2014) The role of the tumor-microenvironment in lung cancer-metastasis and its relationship to potential therapeutic targets. Cancer Treat Rev 40(4):558–566
9. Papotti M, Kalebic T, Volante M, Chiusa L, Bacillo E, Cappia S, Lausi P, Novello S, Borasio P, Scagliotti GV (2006) Bone sialoprotein is predictive of bone metastases in resectable non-small-cell lung cancer: a retrospective case-control study. J Clin Oncol 24(30):4818–4824
10. Zhang L, Hou X, Lu S, Rao H, Hou J, Luo R, Huang H, Zhao H, Jian H, Chen Z, Liao M, Wang X (2010) Predictive significance of bone sialoprotein and osteopontin for bone metastases in resected chinese non-small-cell lung cancer patients: a large cohort retrospective study. Lung Cancer 67(1):114–119
11. Peng X, Guo W, Ren T, Lou Z, Lu X, Zhang S, Lu Q, Sun Y (2013) Differential expression of the RANKL/RANK/OPG system is associated with bone metastasis in human non-small cell lung cancer. PLoS ONE 8(3):e58361
12. Nakamura ES, Koizumi K, Kobayashi M, Saitoh Y, Arita Y, Nakayama T, Sakurai H, Yoshie O, Saiki I (2006) RANKL-induced CCL22/macrophage-derived chemokine produced from osteoclasts potentially promotes the bone metastasis of lung cancer expressing its receptor CCR4. Clin Exp Metastasis 23(1):9–18
13. Chim SM, Qin A, Tickner J, Pavlos N, Davey T, Wang H, Guo Y, Zheng MH, Xu J (2011) EGFL6 promotes endothelial cell migration and angiogenesis through the activation of extracellular signal-regulated kinase. J Biol Chem 286(25):22035–22046
14. Chang CC, Sung WW, Hsu HT, Yeh CM, Lee CH, Chen YL, Liu TC, Yeh KT (2018) Validation of EGFL6 expression as a prognostic marker in patients with lung adenocarcinoma in Taiwan: a retrospective study. BMJ Open 8(6):e021385
15. An J, Du Y, Fan X, Wang Y, Ivan C, Zhang XG, Sood AK, An Z, Zhang N (2019) EGFL6 promotes breast cancer by simultaneously enhancing cancer cell metastasis and stimulating tumor angiogenesis Oncogene 38(12):2123–2134
16. Huo FC, Zhu WT, Liu X, Zhou Y, Zhang LS, Mou J (2021) Epidermal growth factor-like domain multiple 6 (EGFL6) promotes the migration and invasion of gastric cancer cells by inducing epithelial-mesenchymal transition. Invest New Drugs 39(2):304–316
17. Zhu Z, Ni H, You B, Shi S, Shan Y, Bao L, Duan B, You Y (2018) Elevated EGFL6 modulates cell metastasis and growth via AKT pathway in nasopharyngeal carcinoma. Cancer Med 7(12):6281–6289
18. Yeung G, Mulero JJ, Berntsen RP, Loeb DB, Drmanac R, Ford JE (1999) Cloning of a novel epidermal growth factor repeat containing gene EGFL6: expressed in tumor and fetal tissues. Genomics 62(2):304–307
19. Kang J, Wang J, Tian J, Shi R, Jia H, Wang Y (2020) The emerging role of EGFL6 in angiogenesis and tumor progression. Int J Med Sci 17(10):1320–1326
20. Rami-Porta R, Asamura H, Travis WD, Rusch VW (2017) Lung cancer - major changes in the american Joint Committee on Cancer eighth edition cancer staging manual. CA Cancer J Clin 67(2):138–155
21. Salvador F, Llorente A, Gomis RR (2019) From latency to overt bone metastasis in breast cancer: potential for treatment and prevention. J Pathol 249(1):6–18
22. Popper HH (2016) Progression and metastasis of lung cancer. Cancer Metastasis Rev 35(1):75–91
23. Zhang X (2019) Interactions between cancer cells and bone microenvironment promote bone metastasis in prostate cancer. Cancer Commun (Lond) 39(1):76
24. Hirsch FR, Scagliotti GV, Mulshine JL, Kwon R, Curran WJ Jr, Wu YL, Paz-Ares L (2017) Lung cancer: current therapies and new targeted treatments. Lancet 389(10066):299–311
25. Kuchuk M, Kuchuk I, Sabri E, Hutton B, Clemons M, Wheatley-Price P (2015) The incidence and clinical impact of bone metastases in non-small cell lung cancer. Lung Cancer 89(2):197–202
26. Zhang W, Bado IL, Hu J, Wan YW, Wu L, Wang H, Gao Y, Jeong HH, Xu Z, Hao X, Lege BM, Al-Ouran R, Li L, Li J, Yu L, Singh S, Lo HC, Niu M, Liu J, Jiang W, Li Y, Wong STC, Cheng C, Liu Z, Zhang XH (2021) *The bone microenvironment invigorates metastatic seeds for further dissemination* Cell, 184(9): p. 2471–2486.e20
27. Wang X, Yuan W, Wang X, Qi J, Qin Y, Shi Y, Zhang J, Gong J, Dong Z, Liu X, Sun C, Chai R, Le Noble F, Liu D (2016) The somite-secreted factor Maeg promotes zebrafish embryonic angiogenesis. Oncotarget 7(47):77749–77763
28. Zhang G, Chen L, Khan AA, Li B, Gu B, Lin F, Su X, Yan J (2018) *miRNA-124-3p/neuropilin-1(NRP-1) axis plays an important role in mediating glioblastoma growth and angiogenesis* Int J Cancer, 143(3): p. 635–644
29. Park JH, Lee NK, Lee SY (2017) Current understanding of RANK Signaling in Osteoclast differentiation and maturation. Mol Cells 40(10):706–713

30. Macian F (2005) NFAT proteins: key regulators of T-cell development and function. Nat Rev Immunol 5(6):472–484
31. Zhang L, Feng M, Li Z, Zhu M, Fan Y, Chu B, Yuan C, Chen L, Lv H, Hong Z, Hong D (2018) Bulleyaconitine A prevents Ti particle-induced osteolysis via suppressing NF-kappaB signal pathway during osteoclastogenesis and osteoblastogenesis. J Cell Physiol 233(9):7067–7079
32. Brabletz T, Kalluri R, Nieto MA, Weinberg RA (2018) EMT in cancer Nat Rev Cancer 18(2):128–134
33. Zhang Y, Wang X (2020) Targeting the Wnt/beta-catenin signaling pathway in cancer. J Hematol Oncol 13(1):165
34. Martini M, De Santis MC, Braccini L, Gulluni F, Hirsch E (2014) PI3K/AKT signaling pathway and cancer: an updated review. Ann Med 46(6):372–383
35. Peluso I, Yarla NS, Ambra R, Pastore G, Perry G (2019) MAPK signalling pathway in cancers: olive products as cancer preventive and therapeutic agents. Semin Cancer Biol 56:185–195
36. Meurette O, Mehlen P (2018) Notch Signaling in the Tumor Microenvironment. Cancer Cell 34(4):536–548
37. Katso R, Okkenhaug K, Ahmadi K, White S, Timms J, Waterfield MD (2001) Cellular function of phosphoinositide 3-kinases: implications for development, homeostasis, and cancer. Annu Rev Cell Dev Biol 17:615–675
38. Guerrero-Zotano A, Mayer IA, Arteaga CL (2016) PI3K/AKT/mTOR: role in breast cancer progression, drug resistance, and treatment. Cancer Metastasis Rev 35(4):515–524
39. Fattahi S, Amjadi-Moheb F, Tabaripour R, Ashrafi GH, Akhavan-Niaki H (2020) PI3K/AKT/mTOR signaling in gastric cancer: epigenetics and beyond. Life Sci 262:118513
40. Ediriweera MK, Tennekoon KH, Samarakoon SR (2019) Role of the PI3K/AKT/mTOR signaling pathway in ovarian cancer: Biological and therapeutic significance. Semin Cancer Biol 59:147–160
41. Chen H, Zhou L, Wu X, Li R, Wen J, Sha J, Wen X (2016) The PI3K/AKT pathway in the pathogenesis of prostate cancer. Front Biosci (Landmark Ed) 21:1084–1091
42. Iksen S, Pothongsrisit, Pongrakhananon V (2021) *Targeting the PI3K/AKT/mTOR signaling pathway in Lung Cancer: an update regarding potential drugs and Natural Products*. Molecules, 26(13)
43. Mortensen DS, Fultz KE, Xu S, Xu W, Packard G, Khambatta G, Gamez JC, Leisten J, Zhao J, Apuy J, Ghoreishi K, Hickman M, Narla RK, Bissonette R, Richardson S, Peng SX, Perrin-Ninkovic S, Tran T, Shi T, Yang WQ, Tong Z, Cathers BE, Moghaddam MF, Canan SS, Worland P, Sankar S, Raymon HK (2015) CC-223, a potent and selective inhibitor of mTOR kinase: in Vitro and in vivo characterization. Mol Cancer Ther 14(6):1295–1305

Authors and Affiliations

Xiaoting Song[1,2,3] · Xu Cheng[1,2,3] · Xiangang Jin[4] · Shengyu Ruan[1,2,3] · Xianquan Xu[1,2,3] · Feng Lu[4] · Xinhui Wu[1,2,3] · Fangying Lu[1,2,3] · Mingxuan Feng[5] · Liwei Zhang[1,2] · Renshan Ge[3] · Haixiao Chen[1,2] · Zhenghua Hong[1,2] · Dun Hong[1,2]

✉ Zhenghua Hong
0001hzh@163.com

✉ Dun Hong
hongdun@wmu.edu.cn

[1] Department of Orthopedics, Taizhou Hospital of Zhejiang Province Affiliated to Wenzhou Medical University, No.150 Ximen Road, Linhai 317000, Zhejiang, China

[2] Bone Metabolism and Development Research Center, Taizhou Hospital affiliated to Wenzhou Medical University, Linhai, China

[3] Wenzhou Medical University, Wenzhou, China

[4] Taizhou Hospital of Zhejiang Province, Zhejiang University, Linhai, China

[5] Department of Orthopedics, Taizhou Central Hospital affiliated to Taizhou College, Taizhou, China